ACCSCIENCE PUBLISHING

ORIGINAL RESEARCH ARTICLE

An asymmetric dual-layer electrospun membrane with potential for organoid encapsulation and transplantation

Xin Yi[1], Zhihao Pan[1], Yukang Wang[1], Jie Wang[1], Yufei Liu[1], Jie Zhou[1], Jinpeng Wan[1], Yiming Wang[1], Dan Yao[1], Xiaoming Hou[1,2], and Shufang Wang[1]*

[1]Key Laboratory of Bioactive Materials, Ministry of Education, School of Life Sciences, Nankai University, Tianjin, China

[2]Department of Critical Care Medicine, Emergency Medicine Research Institute, Tianjin Fifth Central Hospital, Tianjin, China

***Corresponding author:** Shufang Wang (wangshufang@nankai.edu.cn)

Citation: Yi X, Pan Z, Wang Y, *et al*. An asymmetric dual-layer electrospun membrane with potential for organoid encapsulation and transplantation. *Organoid Res.* doi: 10.36922/OR026380034

Received: September 19, 2026

Revised: October 18, 2026

Accepted: October 26, 2026

Published online: November 26, 2026

Copyright: © 2026 Author(s). This is an Open-Access article distributed under the terms of the Creative Commons Attribution License, permitting distribution, and reproduction in any medium, which provided that the original work is properly cited.

Publisher's Note: AccScience Publishing remains neutral with regard to jurisdictional claims in published maps and institutional affiliations.

Abstract

Organoid transplantation holds great promise for treating various diseases, but its therapeutic potential is limited by insufficient vascularization and host immune rejection. Conventional macroencapsulation strategies often face a fundamental trade-off between immune protection and efficient mass transport, while their fabrication can be complex. Here, we developed a simple, asymmetric, tunable dual-layer electrospun membrane to protect transplanted cells and organoid-derived therapeutic constructs. The membrane was fabricated by sequential electrospinning to generate two layers with distinct pore architectures, inspired by the hierarchical fibrous structure of the native extracellular matrix (ECM). The asymmetric pore structure enables functional separation, with the denser inner layer acting as a physical barrier to host-cell infiltration and promoting tubular structure formation by endothelial cells. Importantly, the fiber diameter and pore size of each layer can be tuned independently, providing flexibility to adapt the membrane to different cell or organoid systems. The ECM-mimetic fibrous architecture exhibited favorable surface wettability and mechanical properties, while maintaining good cytocompatibility. Its extracts promoted human umbilical vein endothelial cells tube formation *in vitro*, while cell-penetration and dextran-permeability assays demonstrated cellular exclusion and size-dependent molecular transport. Fourteen-day subcutaneous implantation indicated good short-term biocompatibility, with no apparent systemic toxicity and a hemolysis rate below 5%. In preliminary pancreatic islet transplantation experiments, encapsulated islets showed improved glycemic regulation compared with unencapsulated islets. Collectively, this asymmetric, tunable, and ECM-mimetic electrospun membrane provides a simple multifunctional platform that balances immune protection, molecular transport, and support for endothelial tube formation, offering potential for cell- or organoid-based transplantation.

Keywords: Asymmetric dual-layer membrane; Electrospun; Islet transplantation; Organoid encapsulation; Extracellular matrix-mimetic

1. Introduction

Cell-based therapies and organoid technologies have emerged as promising approaches for tissue regeneration, disease modeling, and developing therapeutic products.[1] Organoids are three-dimensional, multicellular structures derived from stem or tissue-specific progenitor cells that can recapitulate important aspects of native tissue architecture, cellular composition, and function.[2-4] Beyond their established roles as experimental models, organoids and

organoid-derived cellular constructs are increasingly being investigated as potential therapeutic grafts for tissue repair and regeneration.[5,6] In particular, pancreatic islet organoids and hepatic organoids hold tremendous promise for treating endocrine and metabolic disorders, such as type 1 diabetes and end-stage liver disease.[7–11] However, regardless of whether the therapeutic graft consists of individual cells, cell aggregates, or organoid-derived constructs, the survival and functional maintenance of transplanted cells remain major determinants of therapeutic outcome and are challenged by two interconnected barriers: inadequate vascularization and host immune rejection. Grafts lacking established blood vessels before transplantation are highly susceptible to hypoxia and nutrient deprivation during the early post-transplantation period, which can compromise cell survival and function.[12,13] Simultaneously, allogeneic or xenogeneic transplantation can trigger innate and adaptive immune responses involving macrophages, T lymphocytes, and the complement system, leading to graft injury and fibrotic capsule formation. The resulting inflammatory and fibrotic microenvironment can further restrict oxygen and nutrient transport and disrupt interactions between the transplanted cells and the surrounding extracellular matrix (ECM).[14–18] Thus, inadequate vascularization and immune-mediated injury are not independent obstacles but mutually reinforcing processes that can severely impair the survival, differentiation, and long-term function of transplanted organoids and other cellular constructs, ultimately limiting their therapeutic efficacy. Therefore, developing biomaterial interfaces that can provide structural support, maintain molecular exchange, possess vascularization functions, and protect transplanted cells from adverse host reactions is a crucial step in the successful translation of organoid and cell therapies.

To address these obstacles, various encapsulation strategies have been developed to establish a physical barrier between transplanted cells/organoids and the host immune system, while maintaining adequate mass transfer of nutrients, oxygen, and therapeutic products.[19] Hydrogel microcapsules are among the most widely studied carriers; however, their clinical outcomes have been less than ideal due to issues such as capsule loss, excessive surface fibrosis, and poor mechanical stability under dynamic physiological conditions.[20,21] An alternative strategy is to deliver cells/organoids using macroscopic encapsulation devices, which provide physical protection and can be recovered in the event of adverse events.[22–24] However, these devices suffer from limited loading capacity, poor surface area to volume ratio, and susceptibility to foreign body reactions, ultimately leading to dense fibrotic capsules that impair the long-term function of the graft.[25] The ECM is a crucial component of the cellular microenvironment, providing structural and biochemical signals that regulate cell adhesion, migration, proliferation, differentiation, and tissue structure.[26] During organoid development and tissue regeneration, the interaction between cells and the surrounding ECM plays a vital role in maintaining cell phenotype and tissue structure.[27] Therefore, biomaterials that can provide an ECM-like structural framework can help support cell-material interactions and facilitate the transition from the *in vitro* culture environment to the implanted tissue environment.[28] Electrospun fiber materials are particularly suitable for this purpose because their interconnected fiber networks, high specific surface area, and tunable morphology can reproduce the specific structural features of natural ECMs.[29] This fibrous structure provides a large interface for protein adsorption and cell–cell interactions, while allowing the physicochemical properties of the material to be tuned by controlling fiber diameter, porosity, thickness, and macromolecule composition.[30] These properties make electrospun membranes ideal candidates for constructing biomaterial interfaces that both support transplanted cells and control the interaction between the graft and host tissue.[31,32] Indeed, several studies have demonstrated that electrospun scaffolds support the attachment, proliferation, and differentiation of various cell types, and promote host vascular infiltration by providing topographical cues that guide endothelial cell migration.[33,34]

Despite these advantages, a membrane designed for transplantation must satisfy several requirements.[35] First, transplanted cells need continuous access to oxygen, glucose, nutrients, and other small molecules, while metabolic waste and therapeutic products must be able to diffuse away from the graft.[36] Second, the membrane should limit infiltration of host immune cells and inflammatory cells that may damage the transplanted cells.[37] Third, integration of the implant with the surrounding tissue and the establishment of a vascularized interface are important for improving oxygen and nutrient delivery over time.[38] A dense membrane with small pores may effectively restrict cellular penetration but can increase diffusion resistance, whereas a highly porous membrane may facilitate transport and tissue integration while allowing infiltration of macrophages, fibroblasts, and other host cells.[39] Therefore, the development of multilayer or asymmetric membranes that spatially segregate barrier and permissive functions into distinct layers may provide a rational strategy for balancing these competing requirements.[40] In principle, a relatively compact inner layer can serve as a physical barrier to host-cell infiltration, whereas a more open outer layer can facilitate molecular exchange, protein–material interactions, and tissue integration. Previous studies have demonstrated the feasibility of dual-porosity electrospun membranes for cellular immune isolation and vascularization.[41] More recent biomaterial designs have further emphasized the importance of combining

immunoprotection with pro-angiogenic properties in cell-therapy devices.[42–44] These findings suggest that the biological performance of a transplantation membrane may be improved by spatially assigning different functions to different layers rather than relying on a uniform pore structure. However, many of these designs rely on distinct polymer compositions for each layer, introducing potential interfacial delamination, complex fabrication processes, and inconsistent biological performance due to chemical heterogeneity.[45,46] Nevertheless, simple electrospun polymeric membranes with readily tunable dual-layer architectures remain attractive because they can be fabricated without highly complex processing and may provide a practical balance between structural control, selective transport, cellular exclusion, and host tissue interaction. The complexity of many tissues and organs poses a challenge to traditional tissue engineering methods. Not all tissues are the same, so biomaterials that can be adapted to different tissues are very promising.[26]

In the present study, we developed a simple dual-layer electrospun polymeric membrane with different pore architectures for potential application in the transplantation of therapeutic cellular constructs (**Figure S1**). This membrane was fabricated via a sequential electrospinning strategy using an identical polymer composition for both layers, thereby eliminating chemical incompatibility and ensuring robust interlayer bonding. The design rationale is inspired by the hierarchical organization of native ECM, specifically the dual structure of the dense basement membrane and the loose interstitial stroma, which synergistically provide both barrier function and a permissive microenvironment for cell infiltration and angiogenesis. Our design is based on the hypothesis that spatially differentiated porous structures could provide complementary functions within a single membrane: a relatively compact layer to limit cellular penetration and a more open fibrous layer to facilitate molecular transport and support a favorable tissue-interactive microenvironment. The membrane was first characterized for its chemical composition, surface wettability, mechanical properties, fiber morphology, and pore architecture. Its cytocompatibility was subsequently evaluated using L929 fibroblasts and human umbilical vein endothelial cells (HUVECs). Protein adsorption and cell accumulation on the membrane surface were examined to characterize the material–biological interface, while HUVEC-based assays were used to investigate the pro-angiogenic potential of membrane extracts. The cellular barrier function of the membrane was evaluated using L929 fibroblasts in a Transwell system, and size-dependent molecular transport was investigated using fluorescein isothiocyanate (FITC)-labeled dextrans with different molecular weights. Finally, short-term *in vivo* biocompatibility was assessed following subcutaneous implantation through histological examination of major organs and a hemolysis assay. A pancreatic-islet transplantation experiment was additionally performed to examine the feasibility of applying the membrane to a cellular transplantation model. In summary, this study proposes a biomimetic, structurally asymmetric, and functionally tunable dual-layer electrospun membrane as a candidate for organoid encapsulation and transplantation. By mimicking the hierarchical structure of the natural ECM, this scaffold integrates barrier and permeation functions into a single scaffold. The convenient tunability of fiber diameter and pore size allows for customization for different cell types, organoid systems, or clinical scenarios, extending the platform's applications beyond islet transplantation to include liver, kidney, and neural organoid therapies, providing a potential biomaterial interface for future applications in cell- or organoid-derived therapeutic transplantation.

2. Materials and methods

2.1. Materials, cells and animals

Poly(ε-caprolactone) (PCL; catalog number: 24980-41-4, average M_w: 80, 000) pellets were obtained from Sigma (USA). Collagen type Ⅳ (Col IV) was received from Nacol Biotech Co., Ltd. (China). 1,1,1,3,3,3-hexafluoro-2-propanol (HFIP; catalog number: H811027) was sourced from Macklin Inc. (China). Matrigel (catalog number: NM-G005) was obtained from Novoprotein (China).

Hematoxylin-eosin (H&E; catalog number: G1120) staining kit was purchased from Solarbio Biotechnology Co., Ltd. (China). Cell Counting Kit-8 (CCK8; catalog number: 40203ES60) was sourced from Yeasen Biotechnology Co., Ltd. (China). Calcein-acetoxymethyl ester/propidium iodide Double Stain Kit (catalog number: C2015M) was obtained from Beyotime Biotechnology Co., Ltd. (China).

Male BALB/c mice (six- to eight-week-old; n = 42) and Sprague Dawley rats (weighing 250 ± 50 g; n = 32) were purchased from the SPF (Beijing) Biotechnology Co., Ltd. (China). HUVECs were purchased from Zhong Qiao Xin Zhou Biotechnology Co., Ltd. (China).

2.2. Fabrication of the electrospun membranes

2.2.1. Fabrication of the Inner-layer electrospun membrane

Typically, 0.9 g PCL and 0.1 g Col Ⅳ were dissolved in 10 mL HFIP and stirred at room temperature for 24 h with a magnetic stirrer to ensure full dissolution. The electrospinning technique was employed to produce the membranes. The parameters for fabricating the inner-layer electrospun membrane included a voltage of 17 kV, a distance from the syringe needle tip to the collector of 17 cm, and a flow rate of 0.5 mL/h. The Electrospinning

process lasted for 5 h through a 30-gauge blunt needle, with the temperature at room temperature and the relative humidity at 45 ± 5%.

2.2.2. Fabrication of the outer-layer electrospun membrane

Specifically, 1.35 g PCL and 0.15 g Col Ⅳ were dissolved in 10 mL HFIP, stirred at room temperature for 24 h, and electrospun at 15 kV through a 21-gauge blunt needle, which served as the spinneret. The polymer solution was fed at a flow rate of 2 mL/h, with the spinneret-to-mandrel distance set to 15 cm, the temperature at room temperature, and the relative humidity at 45 ± 5%. The electrospinning process lasted for 70 min.

2.2.3. Fabrication of the dual-layer electrospun membrane

After the inner-layer electrospun membrane was prepared, the outer-layer electrospun membrane was prepared while the HFIP solvent was not completely evaporated, resulting in a dual-layer electrospun membrane.

2.2.4. Fabrication of transplantation devices

A 1 cm diameter polytetrafluoroethylene ring mold heated to 60℃ and pressed onto an electrospun membrane was used to bond two membranes together, preserving the internal space to encapsulate cells or organoids. The bonded portion was then cut off to obtain a circular cell transplantation device. For islet transplantation, 500 Islet Equivalent Quantity units were encapsulated within each device.

2.3. Characterization of the electrospun membranes

Electrospun membranes were cut into 1 × 1 cm^2 squares and sputter-coated with gold; their microstructures were examined using scanning electron microscopy (QUANTA 200, FEI Company, Czech Republic). Images were captured using a color charge-coupled device camera. For each experimental group, three samples were prepared, and three random fields of view were selected per sample. ImageJ software (1.54t, National Institutes of Health, USA) was used to measure fiber diameters and pore sizes ($n = 40$). The chemical structure of electrospun membranes with and without collagen was analyzed by Fourier transform infrared (FTIR) spectroscopy. The dried membranes were cut into 1 × 3 cm^2 strips, and their thicknesses were measured and recorded (inner layer: 32.33 ± 2.42 μm; outer layer: 90.33 ± 2.16 μm; dual-layer: 103.8 ± 2.14 μm, $n = 6$) prior to tensile testing. A tensile machine (3345, Instron, USA) was employed to assess the tensile properties of the membranes at a tensile speed of 10 mm/min. Each test was repeated six times. The water contact angles of the membranes were determined using a contact angle measuring instrument (HARKE-SPCA, Beijing Hako Testing Instrument Factory, China). This experiment was performed in triplicate, with six parallel replicates for each run.

2.4. Cytocompatibility

2.4.1. Cell Counting Kit-8 assay

Preparation of membrane extracts was as follows: 6 cm^2 membrane (Inner-layer, Outer-layer, or Dual-layer) was immersed in 1 mL of RPMI-1640/Dulbecco's Modified Eagle Medium basic medium and shaken on a shaker at 37°C for 24 h. The extractions were sterilized through 0.22 μm-pore-size filters and refrigerated at 4℃ for subsequent experiments. The experimental groups were as follows: Control group (cells without any extract), Inner group (cells cultured using the inner-layer electrospun membrane extract), Outer group (outer-layer electrospun membrane extract), Dual group (dual-layer electrospun membrane extract).

L929 cells were seeded in 96-well plates (3×10^3 cells/well) and cultured in RPMI-1640 medium (GIBCO, USA) with 10% fetal bovine serum (FBS) supplemented at 37℃ for 24 h. HUVECs were seeded at the same density in 96-well plates and incubated in HUVEC medium at 37℃ for 24 h. Then, medium prepared from the extracts was used to continue culturing cells for 1, 2, and 3 days. CCK8 solution was added to each well and incubated for 2 h. Finally, the microplate reader (iMark, Bio-Rad, USA) was used to measure the absorbance at 450 nm. The experiment was performed in triplicate, with three technical replicates for each group.

2.4.2. Live/dead staining

L929 cells/HUVECs were seeded at a density of 8×10^4 cells/mL on confocal dishes with medium prepared from the extracts and cultured for 48 h. At room temperature, calcein-acetoxymethyl ester solution, propidium iodide solution, and buffer were mixed at a ratio of 1:1:1,000 to prepare a working solution. After washing away residual medium with phosphate-buffered saline (PBS), the working solution was added. Cells were observed and photographed using a laser scanning confocal microscope (TCS SP5, Leica, Germany), and the number of live and dead cells was counted using ImageJ software. This experiment was performed in triplicate, with three randomly selected fields of view imaged for each replicate.

2.5. Surface properties

2.5.1. Protein adhesion assay

The FITC-bovine serum albumin (BSA) at a concentration of 0.5 mg/mL was introduced to assess protein adhesion levels in the control group (electrospun membrane containing only PCL) and the experimental groups (Inner, Outer, and Dual). Electrospun membranes cut into 1 ×

1 cm^2 pieces were immersed in 200 μL of a 0.5 mg/mL FITC-BSA solution and incubated for 4 h in the dark. After incubation, excess FITC-BSA was washed away with PBS, and the membranes were then observed under a confocal microscope. This experiment was performed in triplicate with three randomly selected fields of view for each condition.

2.5.2. In vivo cell deposition staining

All animal experiments were approved by the Animal Ethics Committee of Nankai University and conducted in strict accordance with the National Research Council's Guide for the Care and Use of Laboratory Animals. Circular devices made from electrospun membranes were implanted subcutaneously on the backs of balb/c mice (n = 6 per group; four groups in total). After 14 days, the devices were removed and subjected to frozen sectioning and H&E staining. Cell deposition on the membrane surface was observed under a microscope, and the thickness of the cell deposition layer was measured and calculated using ImageJ software.

2.6. Angiogenesis assay

Matrigel was added to 24-well plates (30 μL/well) and spread out, then allowed to flow and level overnight at 4°C, and incubated at 37°C for 2 h to solidify. HUVECs were seeded onto the Matrigel at 1×10^5 cells/100 μL of culture medium, followed by the addition of the membrane extracts. After 4 h of incubation, images were acquired by randomly selecting fields of view under an optical microscope. This experiment was performed in triplicate, with three technical replicates for each condition. The number of nodes and total vessel length were quantitatively analyzed using ImageJ software.

2.7. Selective permeability

2.7.1. Cell permeability assay

L929 cells were utilized to test the cell permeability of the membranes. The membranes sterilized by ultraviolet light were cut into 1×1 cm^2 pieces and then placed at the bottom of Transwell chambers in 24-well plates, as previously reported.[47] 2×10^4 cells in 200 μL medium with 2% FBS were introduced into the chambers with and without membranes, incubated for 24 h, and then the membranes were removed. The cells were fixed with 4% paraformaldehyde and stained with crystal violet ammonium oxalate (Solabio, China). To assess cells that migrated into the basolateral compartment, cells were observed with an optical microscope and counted using ImageJ software. This experiment was performed in triplicate, with three technical replicates for each trial.

2.7.2. Dextran permeability assay

Membrane permeability was determined using a two-compartment system. The dual-layer membrane was fixed between the donor and acceptor compartments, with two interconnected compartments serving as control groups. FITC-dextran of different molecular weights (10, 40, 70, 150 kDa) was added to 100 μL in the upper compartment at 1 mg/mL, while 900 μL of ultrapure water was added to the lower compartment. At selected time intervals (0.5, 1, 2, 4, 8, 12, 24, 48 h), 50 μL of solution was taken from the acceptor compartments, and the fluorescence intensity ratios of the solutions in the acceptor compartments to the control groups were analyzed to determine the amount of permeated solutes. This experiment was performed in triplicate, with three technical replicates for each group.

2.8. *In vivo* islet transplantation and blood glucose regulation

2.8.1. Rat pancreatic islet isolation

Rat pancreatic islets were isolated from Sprague Dawley rats (weighing 250 ± 50 g) using a previously established enzyme digestion procedure.[48] First, 7.5 mg collagenase P (Roche, Germany) was dissolved in 10 mL ice-cold Hank's balanced salt solution (Solabio, China) within 100 μL 750 mM $CaCl_2$ solution and 100 μL HEPES buffer solution (GIBCO, USA). Then, the pancreas, filled by injecting collagenase P solution through the pancreatic duct, was excised from the associated body parts and incubated at 37℃ for 15 min. Afterward, to terminate the enzymatic digestion, 50mL of ice-cold RPMI-1640 medium supplemented with 5% FBS was added. The resulting tissue pellet was washed with RPMI-1640 Medium and filtered through 1.4 mm and 500 μm sieves in sequence. Islets were purified via a density gradient as follows: RPMI-1640 medium/Histopaque 1077 (Sigma, USA)/Histopaque 1119 (Sigma, USA). Finally, to achieve higher purity, the islets were picked manually under a light microscope (CKX53, Olympus, Japan).

2.8.2. Establishment of a diabetic mouse model and islet transplantation

First, a diabetic mouse model was established by inducing healthy balb/c mice with an intraperitoneal injection of streptozotocin (60 mg/kg); mice with random blood glucose levels exceeding 16.7 mM were classified as diabetic. Subsequently, mice were randomly assigned to three groups using randomized block randomization (n = 5 per group). Under sodium pentobarbital anesthesia (30 mg/kg), the mice received different treatments: the diabetic group received no treatment; the naked islet group received an implantation of 500 Islet Equivalent Quantity of unencapsulated islets into the dorsal region; and the encapsulation group received an implantation of a circular islet encapsulation device (approximately 12 mm in diameter), the fabrication of which is described in **Section 2.2.4**. Blood glucose levels were monitored following the surgery.

2.9. Biocompatibility

2.9.1. Hemolysis test

To evaluate the hemocompatibility of the membranes, a hemolytic activity assay was performed. Briefly, rat blood samples were collected and centrifuged at 3,000 rpm for 20 min. The lower erythrocytes were washed five times by resuspending them in PBS and centrifuging. Subsequently, extracts from the electrospun membranes were mixed with the erythrocytes and incubated at 37°C for 1 h, then centrifuged at 3,500 rpm for 15 min. Using physiological saline as a negative control and 0.1% Triton X-100 solution as a positive control, hemolysis was observed and photographed in each group, and supernatant absorbance was measured at 540 nm using a microplate reader. This experiment was conducted in triplicate.

2.9.2. Systemic biocompatibility

The electrospun membrane devices were surgically implanted into the subcutaneous dorsal region of mice. At 14 d post-implantation, the animals were euthanized, and the major organs, including the heart, liver, spleen, lungs, and kidneys, were carefully harvested. The harvested tissues were immediately fixed in 4% paraformaldehyde for 24 h, then were dehydrated through a graded ethanol series (50% to 100%) and embedded in paraffin wax. The paraffin-embedded tissues were sectioned using a rotary microtome. For histological evaluation, the sections were dewaxed, rehydrated, and stained with H&E. Finally, the implanted device was observed under an optical microscope to assess its systemic biocompatibility.

2.10. Statistical analysis

Data are analyzed as mean ± standard deviation for $n \geq 3$. Analysis of variance (one-way or two-way depending on data set) and *t*-test were used to compare more than two means. The data were considered statistically significant when $p \leq 0.05$ ($^{*}p \leq 0.05$, $^{**}p \leq 0.01$, $^{***}p \leq 0.001$, and $^{****}p \leq 0.0001$). All graphs and statistical analyses were performed using GraphPad Prism (version 8.0.1, GraphPad Software, Inc., USA) and ImageJ.

3. Results

3.1. Morphological characterization and quantitative analysis of the electrospun membranes

To prepare a dual-pore-size membrane, we used PCL and Col IV as base materials and fabricated it *via* continuous electrospinning. First, a relatively dense inner-layer membrane was prepared, followed by a looser outer-layer membrane, before solvent evaporation, to achieve a dual-layer electrospun membrane with asymmetric pore sizes. This method is simple and economical. The resulting membrane was characterized by scanning electron microscopy. Analysis showed that the membrane is an interconnected asymmetric pore membrane with two distinct structures on both sides (Figure 1A): the inner layer exhibited a dense, compact fiber network with minimal fiber spacing, while the outer layer exhibited a loose structure with coarser fibers. Both sides of the membrane were randomly oriented and had extensive open pores (Figure 1B).

Quantitative morphometric analysis was performed using ImageJ software on 40 randomly selected fibers and pores per layer. The fiber diameter distribution (Figure 1C, E) showed that the inner layer consisted of significantly finer fibers (average diameter 0.13 ± 0.02 μm), while the outer layer consisted of coarser fibers (average diameter 0.5 ± 0.08 μm). Correspondingly, the pore size distribution also showed significant differences (Figure 1D, F). The inner layer had an average pore size of 0.9 ± 0.18 μm, less than 1 μm, effectively blocking the infiltration of immune cells[49], while the outer layer had much wider pores, with an average pore size of 2.7 ± 0.17 μm, and did not impede the exchange of oxygen and nutrients.[50]

These quantitative data confirm that we have successfully constructed a dual-layer membrane with a dense microporous inner layer and a macroporous outer layer, exhibiting significantly different pore structures. This provides the structural basis for its differentiated barrier and permeation functions. As a fibrous network with specific pore structures, the natural ECM controls substance transport, cell migration, and immune surveillance. Our membrane possesses a unique asymmetric pore structure that remarkably reproduces the dual structural features of the natural basement membrane and its underlying stroma.[51] By adjusting the spinning conditions and changing the filament diameter and pore size of the inner and outer layers (e.g., **Figure S2**), it is possible to mimic the ECM of different tissues.

3.2. Physicochemical properties of the electrospun membranes

The successful electrospinning of PCL with Col Ⅳ had been preliminarily validated using FTIR. As shown in Figure 2A, the FTIR spectrum of the electrospun membrane exhibited characteristic absorption bands at 3,300 cm^{-1} (amide A, N–H stretching vibration), 1,640 cm^{-1} (amide I, C=O stretching vibration), and 1,530 cm^{-1} (amide II, N–H bending vibration), which are typical of the Col Ⅳ backbone.

The hydrophilicity/hydrophobicity of materials significantly influences cell adhesion, growth, proliferation, and other cellular behaviors. Hydrophilic surfaces can improve the affinity of materials for cells and tissues.[52] In this study, the static water contact angle (WCA) was measured at room temperature using the sessile drop

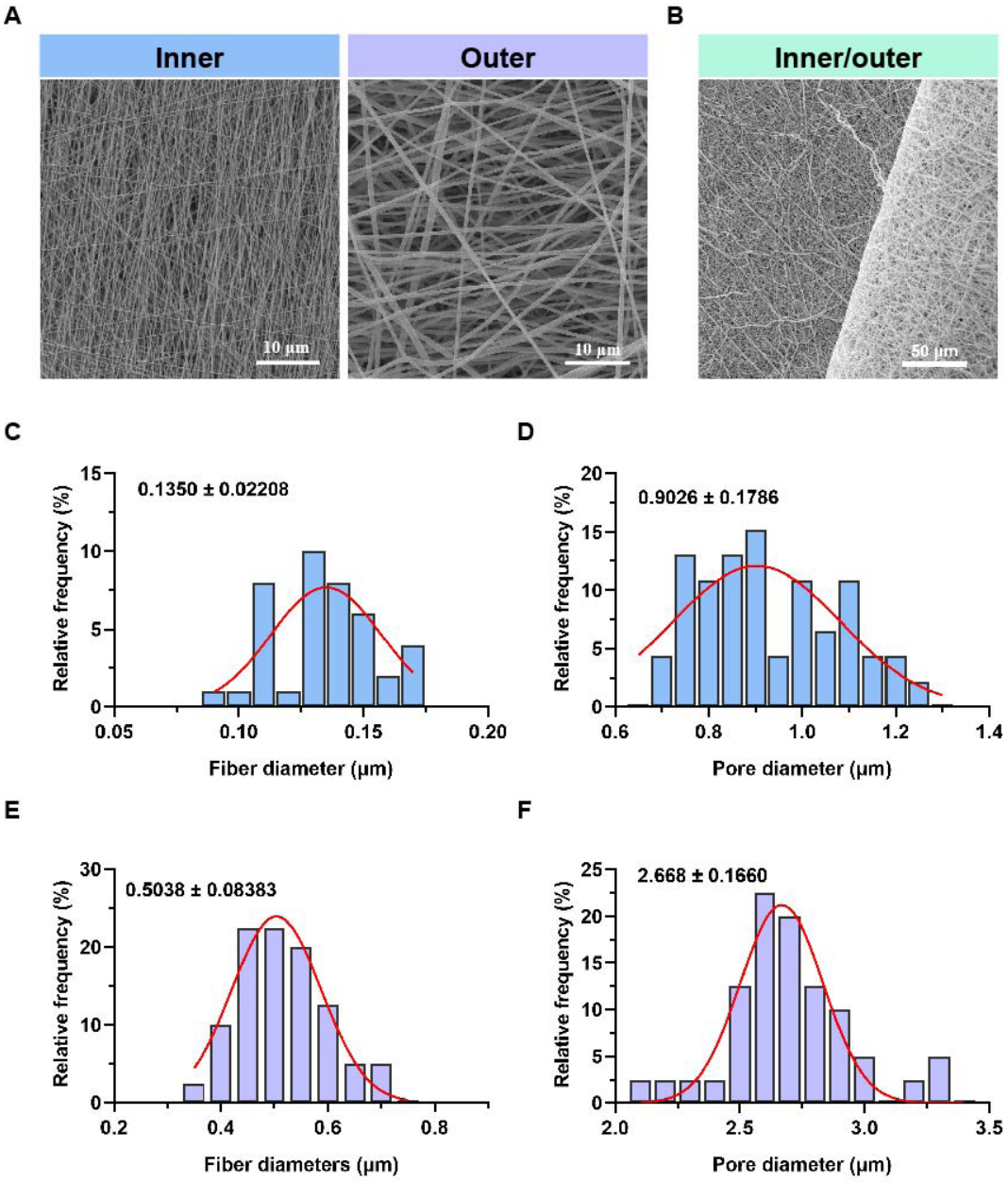

Figure 1. Morphological and characterization analysis of poly(ε-caprolactone)/collagen type Ⅳ electrospun membranes. (A) Microstructure of the electrospun membranes. Scale bars: 10 μm; magnification: 5,000×. (B) Microstructure at the interface between the inner and outer layers of the dual-layer electrospun membrane. Scale bar: 50 μm; magnification: 1,000×. Statistical analysis of (C) fiber diameter and (D) pore diameter in the inner-layer electrospun membrane. (E) Fiber diameter and (F) pore diameter in the outer-layer electrospun membrane (n = 40).

method to evaluate the improvement in hydrophilicity of the inner and outer layers after Col Ⅳ introduction. The electrospun membrane with only PCL had a water contact angle (WCA) value of 106.0° ± 2.15°, while the inner-layer membrane with Col Ⅳ had a WCA value of 43.51° ± 1.36°, and the outer-layer membrane had a WCA value of 38.26° ± 1.05° (n = 6 independent samples, Figure 2B). This highly hydrophilic microenvironment is theoretically favorable for the initial adhesion and spreading of anchorage-dependent cells such as fibroblasts and endothelial cells.[53]

Appropriate mechanical properties ensure that the electrospun membrane maintains a stable morphology during cell encapsulation and transplantation. The mechanical strength of the electrospun membrane was evaluated under uniaxial tensile load using a universal testing machine. A schematic diagram of the tensile

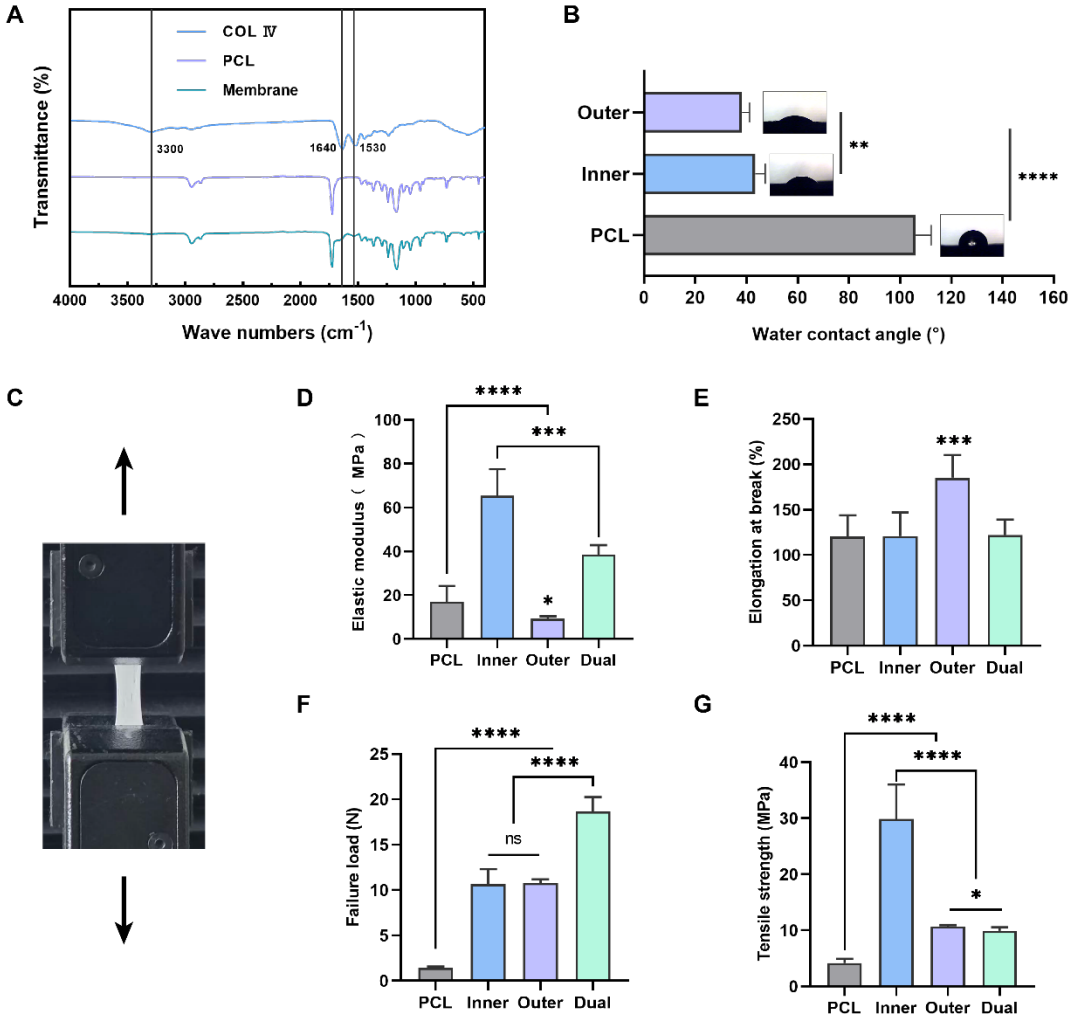

Figure 2. Physicochemical characterization and mechanical properties of the electrospun membranes. (A) Fourier transform infrared analysis of poly(ε-caprolactone) (PCL), collagen type IV (Col Ⅳ), and the dual-layer electrospun membrane. (B) Macroscopic images and statistical results of water contact angle ($n = 6$). (C) Schematic illustration of the tensile testing setup. Mechanical properties of the electrospun membranes, including (D) elastic modulus, (E) elongation at break, (F) failure load, and (G) tensile strength ($n = 6$).
Notes: $^{*}p < 0.05$; $^{***}p < 0.001$; $^{****}p < 0.0001$; ns: not significant.

testing apparatus was shown in Figure 2C. The mechanical properties of each single-layer and dual-layer composite membrane were summarized in Figure 2D–G. The inner layer exhibited the highest elastic modulus and tensile strength in all groups, attributed to its dense fibrous structure. In contrast, the outer layer, due to its porous and loose network structure, exhibited the largest elongation at break, demonstrating excellent flexibility and ductility. Notably, the failure load of the dual-layer composite membrane was higher than that of any single-layer or pure PCL membrane, indicating that beyond the increase in failure load resulting from greater thickness, its rigid inner layer bore the initial tensile stress, while the flexible outer layer absorbed the large deformation energy through deformation buffering, thus preventing sudden fracture of the composite membrane. No interfacial delamination or premature failure was observed at the interface between the two layers throughout the tensile process. These mechanical properties meet the requirements for subcutaneous implantation, and the scaffold is able to withstand manipulation and physiological movement without tearing.[54]

3.3. *In vitro* cytocompatibility of the electrospun membranes

To assess the cell compatibility of the electrospun membranes, L929 cells and angiogenesis-associated HUVECs were used. Live/dead cell staining and the CCK8 assay verified the harmlessness of the electrospun membranes to cell growth and proliferation.

Representative fluorescence micrographs of live/dead cell staining with calcein-acetoxymethyl ester and propidium iodide (Figure 3A: L929 cells; Figure 3D: HUVECs) showed that green fluorescent live cells almost completely covered the bottom of the dish, with only a small number of red fluorescent dead cells randomly scattered. Comparative analysis of green and red fluorescence intensities using ImageJ, as shown in Figure 3B and E, revealed that the survival rates of both L929 cells and HUVECs were above 80%, indicating good cell compatibility of the electrospun membranes.

The proliferation capacity of the seeded cells was further assessed at 24, 48, and 72 h using the CCK8 kit. As shown in Figure 3C and F, the optical density values of both L929 cells and HUVECs at 450 nm increased significantly from day 1 to day 3. Compared with the control group, the Inner, Outer, and Dual groups significantly promoted L929 cell proliferation and had no significant effect on HUVEC proliferation. These results confirmed that the electrospun membranes could maintain short-term cell proliferation, meeting the basic biocompatibility requirements for subsequent *in vivo* studies.

3.4. Transplant protection function of the electrospun membranes

3.4.1. Surface properties of electrospun membranes and enhancement of in vitro tubular structure formation by membrane extracts

The FITC-conjugated BSA (FITC BSA, 0.5 mg mL−1 in PBS) was used as a model protein to examine non-specific protein adsorption on the membrane surface. After static incubation for 4 h, the membranes were thoroughly rinsed and imaged using a fluorescence microscope under consistent fluorescence intensity settings. As shown in Figure 4A, the fluorescence intensity of the Col Ⅳ-containing membranes was significantly lower than that of the positive control PCL membrane. The reduced BSA adsorption on collagen-incorporated membranes compared to pure PCL arises from multiple synergistic factors. Based on existing literature, we hypothesize the following mechanisms: PCL, being hydrophobic, promotes strong hydrophobic interactions with BSA, causing extensive protein deposition. In contrast, collagen enhances surface hydrophilicity, diminishing the thermodynamic driving force for BSA binding. Additionally, collagen

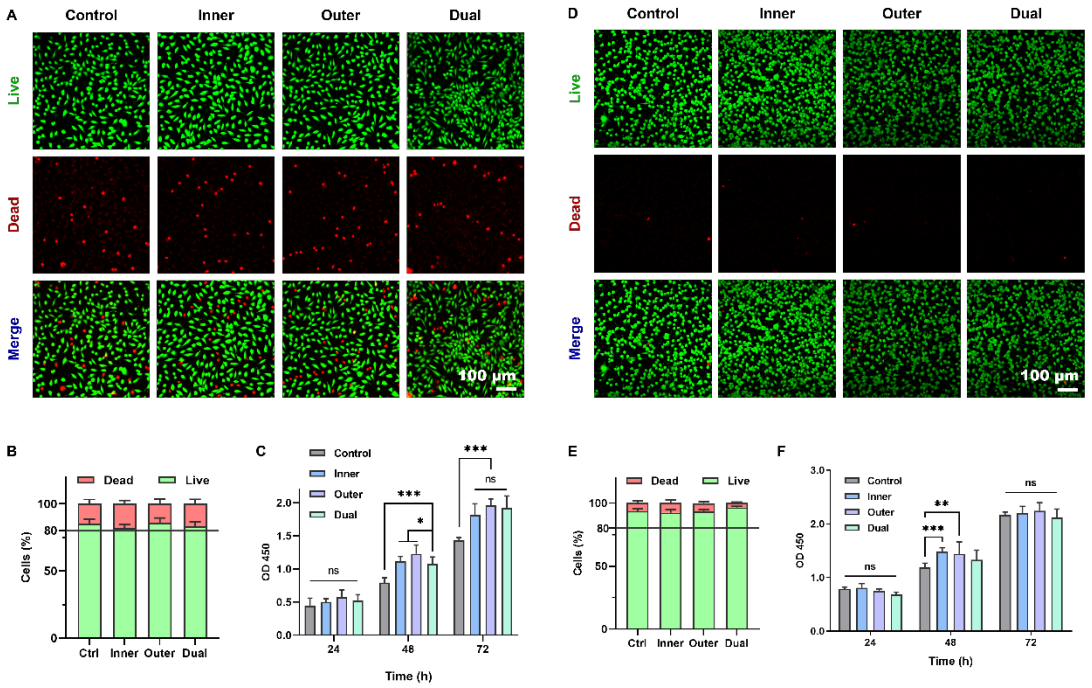

Figure 3. *In vitro* cytocompatibility of the electrospun membranes. (A) Live/dead staining results of L929 cells in different electrospun membrane extracts. Scale bar: 100 μm; magnification: 10×. (B) Quantitative statistics of live/dead staining results. (C) CCK-8 results of L929 cells after 3 days (n = 3). (D) Live/dead staining results of HUVECs (n = 3). Scale bar: 100 μm; magnification: 10×. (E) Quantitative statistics of live/dead staining results (n = 3). (F) CCK-8 results of HUVECs after 3 days (n = 3).
Notes: $^{*}p < 0.05$; $^{**}p < 0.01$; $^{***}p < 0.001$; ns: not significant.

competes with BSA for limited adsorption sites and forms a shielding protein corona that blocks hydrophobic domains.[55,56] Under physiological pH, the negative charges on both collagen and BSA may further impose electrostatic repulsion. Collectively, the synergistic effects of enhanced wettability, competitive adsorption, corona shielding, and charge repulsion are likely reasons for the reduced adhesion of BSA to collagen-containing membranes. These results indicate that the electrospun membrane has excellent anti-protein contamination properties, which is beneficial in reducing the risk of excessive foreign body reaction and thrombosis during implantation.

To investigate cell deposition on the membrane surfaces after *in vivo* transplantation, the devices made from the electrospun membranes were transplanted into the back of mice. After 14 d, sections were prepared and H&E stained, as shown in Figure 4B (the parts within the dashed lines are the electrospun devices). Compared with the positive control PCL membrane, the cell thickness deposited on the inner, outer, and dual-layer electrospun membranes was significantly lower, and the number of cells penetrating into the inner side of the dual-layer membrane was the lowest. The thicknesses of cell deposition on the surfaces were measured and statistically analyzed (Figure 4D). It was found that the thickness in all three experimental groups was lower than that in the control group, but the deposition thickness of the dual-layer membrane was slightly higher than that of the inner-layer membrane, and both were significantly higher than that of the outer-layer membrane. This may be because the outer-layer membrane is more hydrophilic, which is less conducive to cell adhesion.

The effect of membrane extracts on HUVEC tube formation was assessed *in vitro*. To ensure consistent extract concentrations across groups, the membrane extracts were prepared using the method described in **Section 2.4.1**. After 4 h of culture in conditioned medium, the dual-layer membrane extract group showed the best angiogenesis trend, with more branching points and loops, as shown in Figure 4C. Quantitative analysis of the number of nodes and total vessels length using the ImageJ angiogenesis analyzer plugin showed that the total vessels length of the dual-layer membrane group was 1,165 ± 76.52 μm, significantly higher than that of the control group (569.3 ± 52.12 μm, $p \leq 0.01$); the number of nodes was 52.67 ± 1.856, while that of the control group was 36.00 ± 0.5774 ($p \leq 0.01$). These results indicate that Col Ⅳ within the membranes promotes the assembly of endothelial cells into tubular structures *in vitro*. It possesses the potential to facilitate endothelial cell assembly into vascular networks, thereby creating a pro-angiogenic microenvironment.

3.4.2. Immune isolation and size-selective permeability of the dual-layer membrane

We investigated the functional significance of asymmetric pore structures through two complementary experiments: a cell transmembrane permeation experiment in a Transwell system and a macromolecular permeation experiment using FITC-dextran of different molecular weights. These experiments verified that the inner-layer membrane with smaller pore size plays a greater role in blocking the passage of cells and macromolecules.

In the Transwell experiment, we laid electrospun membranes flat in the upper chamber of a 24-well Transwell chamber with a pore size of 8 μm. L929 fibroblasts were seeded in the upper chamber. After 24 h of incubation, cells that migrated to the surface of the chamber were fixed, stained with crystal violet, and counted under a light microscope in at least six random fields of view for each insertion plate. Schematic diagrams of the experiment are shown in Figure 5A.

The results showed that, compared with the control group without electrospun membranes, only an extremely small number of cells penetrated the membranes and landed on the upper surface of the chamber in the two groups with inner-layer and dual-layer electrospun membranes. In the group with the outer-layer membrane, some L929 fibroblasts still penetrated the membrane (Figure 5B). All three groups with electrospun membranes significantly reduced cell penetration (Figure 5C), indicating that inner-, outer-, and dual-layer electrospun membranes all have some anti-cell-migration function.

Meanwhile, we evaluated the permeability of the electrospun membranes to molecules of different sizes using FITC-labeled dextrans (molecular weights of 10 kDa (Stokes radius approximately 2.4 nm), 40 kDa (approximately 4.5 nm), 70 kDa (approximately 5.9 nm), and 150 kDa (approximately 8.5 nm), as shown in Figure 5D.

The cumulative permeation curves (Figure 5E–H) exhibited size selectivity. For the smaller molecular weight dextrans (10 kDa and 40 kDa), the permeability was relatively high, exceeding 50% within 4 h, indicating that small-molecule nutrients could easily pass through the electrospun membranes. The permeability of 70 kDa dextran is less than 50% within 48 hours, while that of 150 kDa dextran is less than 20%. Notably, the permeation curves showed a sharp decrease between 40 kDa and 70 kDa, indicating that the apparent molecular weight cutoff ranged from 50 to 70 kDa. These quantitative permeability data, combined with cellular permeability results, demonstrate that this asymmetric dual-layer membrane acts as a barrier,

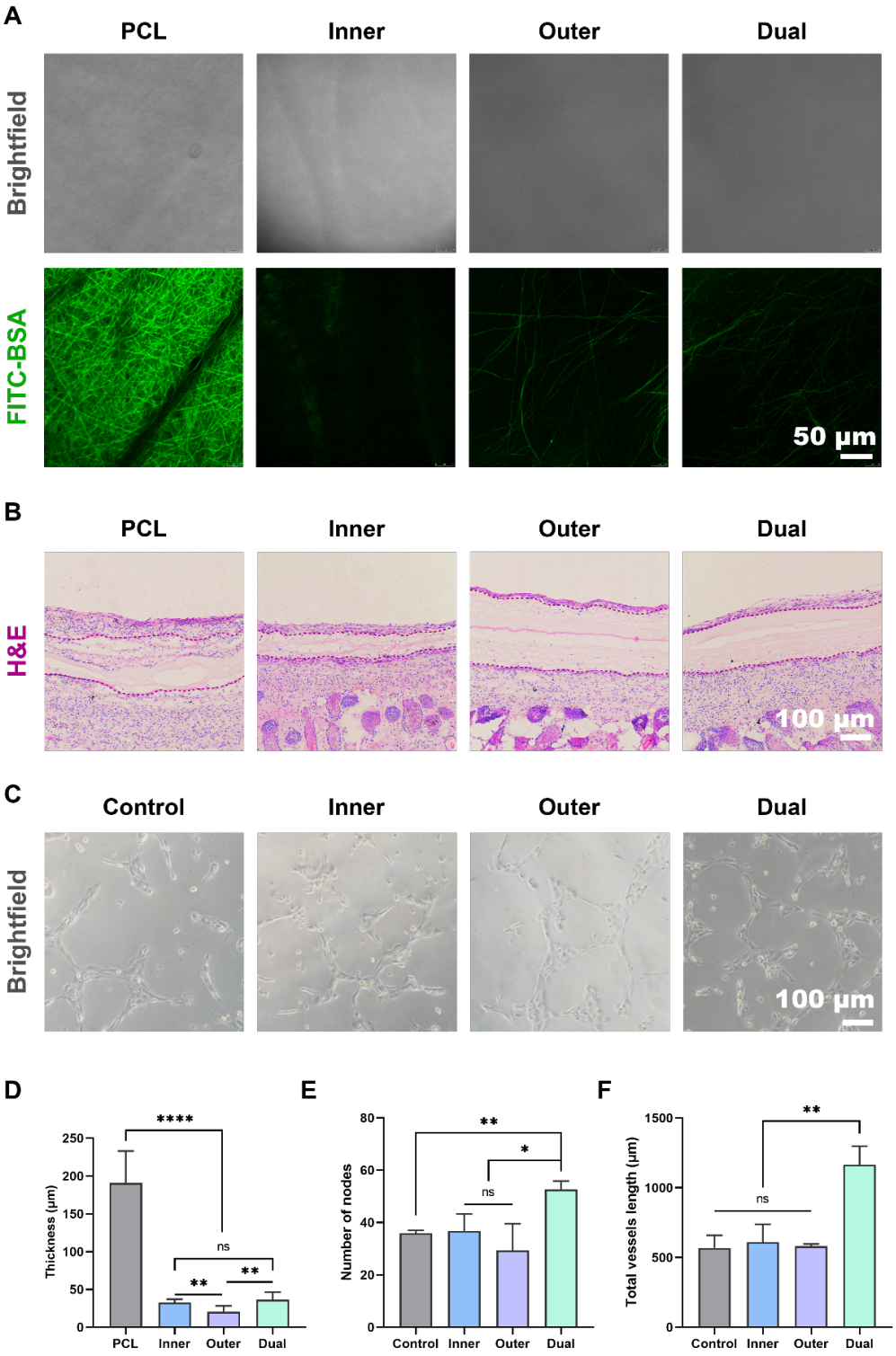

Figure 4. *In vitro* and *in vivo* anti-adhesion function and *in vitro* angiogenesis function of electrospun membranes. Protein adhesion, *in vivo* cellular deposition, and effects of the membranes' extracts on angiogenesis in HUVECs. (A) Protein adhesion images of each group of materials. Scale bar: 50 μm; magnification: 20×. (B) *In vivo* cellular deposition. Scale bar: 100 μm; magnification: 10×. (C) Images of the tube formation assay. Scale bar: 100 μm; magnification: 10×. Quantitative analysis, including (D) semi-quantitative analysis of the thickness of *in vivo* cellular deposition (n = 3), (E) number of nodes, and (F) total vessel length (n = 3).

Abbreviations: BSA: Bovine serum albumin; FITC: Fluorescein isothiocyanate; H&E: Hematoxylin-eosin; HUVECs: Human umbilical vein endothelial cells; PCL: Poly(ε-caprolactone).

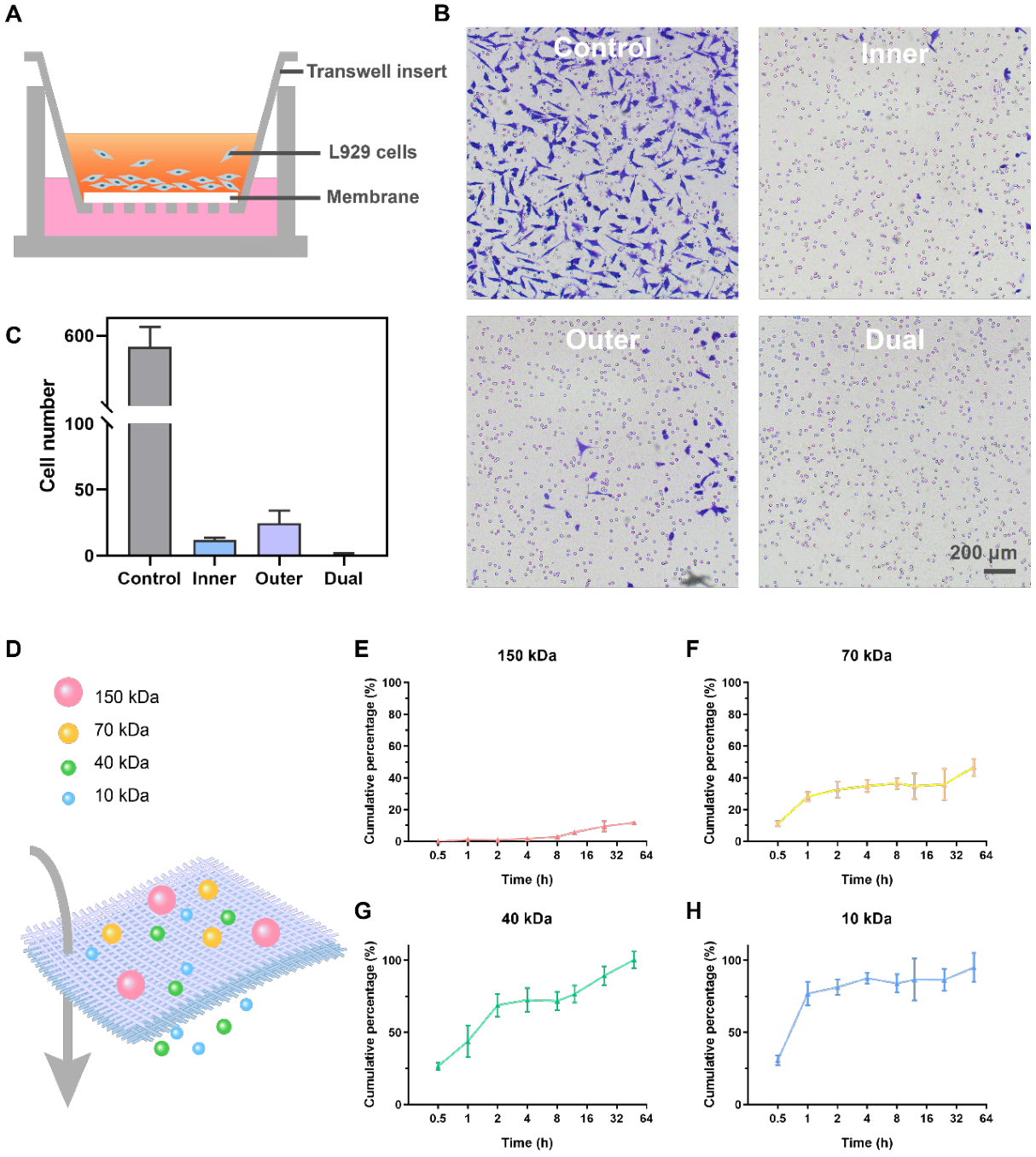

Figure 5. Layer-dependent cellular barrier penetration evaluated via Transwell assay and size-selective permeability of the Dual-layer membrane assessed using FITC-dextran of different molecular weights. (A) Schematic diagram of the membranes blocking L929 cells in the chambers. (B) Images of L929 blocked by the membranes. Scale bar: 200 μm; magnification: 4×. (C) Quantitative analysis ($n = 3$). (D) Schematic diagram of the Dual-layer membrane. Cumulative percentage-time images of dextran permeation solutions with molecular weights of (E) 150 kDa, (F) 70 kDa, (G) 40 kDa, and (H) 10 kDa ($n = 3$).

allowing free exchange of small-molecule nutrients and metabolic waste while effectively restricting the passage of macromolecules and cellular components through its dense inner layer.

3.4.3. Rat islet transplantation and blood glucose regulation

In vivo experimental data using primary rat islet transplantation also confirmed the protective function

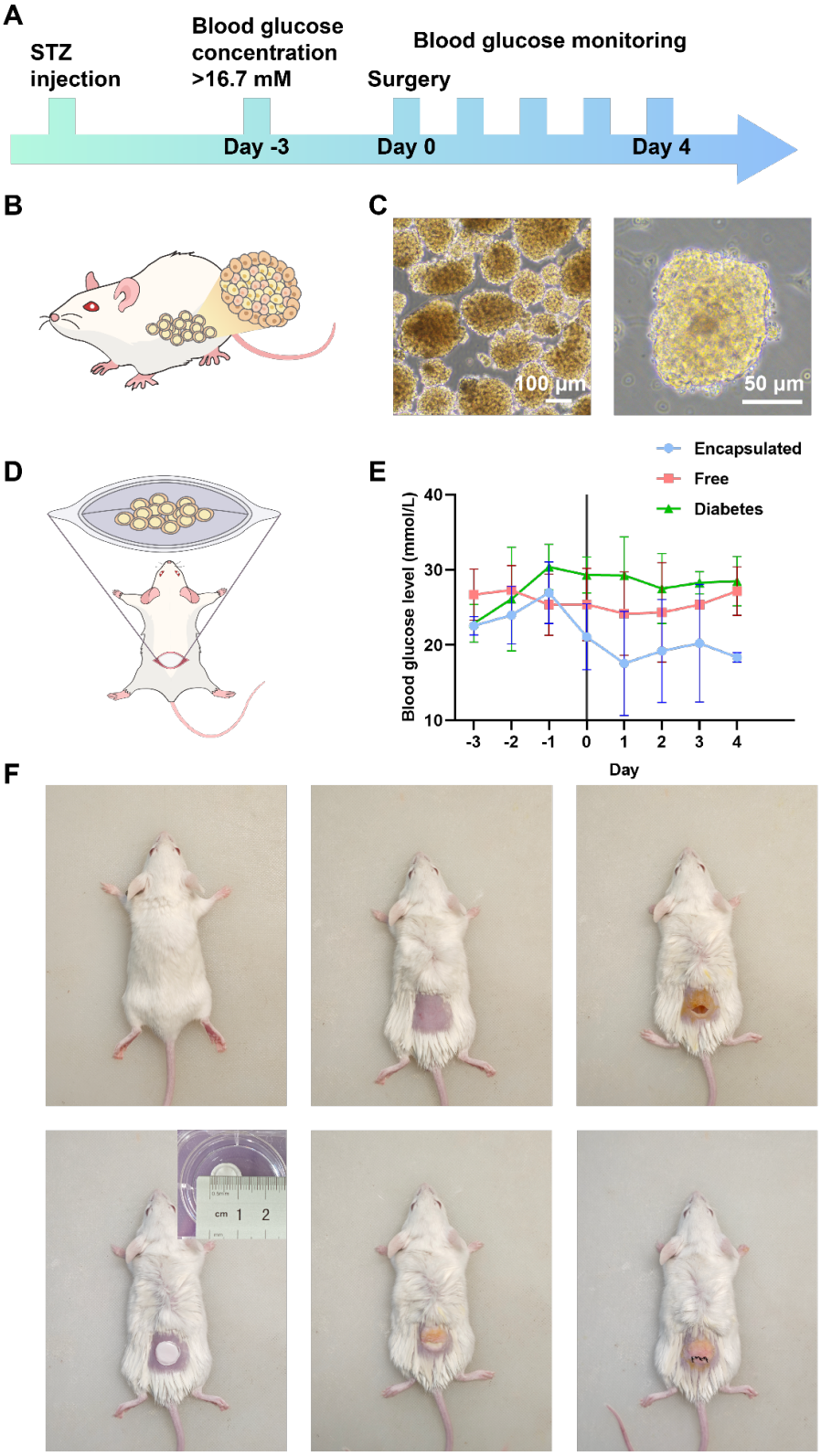

Figure 6. Rat islet extraction and transplantation. (A) Surgical timeline diagram. (B, C) Schematic diagram of rat pancreatic islets and their gross appearance under bright field. Scale bars: 100 μm, 50 μm; magnifications: 10×, 40×. (D, F) Diagram and surgical photograph of subcutaneous transplantation on the back of a mouse. (E) Blood glucose fluctuation monitoring before and after islet transplantation (n = 5).
Abbreviation: STZ: Streptozotocin.

and permeability of the dual-layer electrospun membrane (Figure 6). Compared with free islets, islets encapsulated within the dual-layer electrospun membrane significantly controlled and improved blood glucose levels in mice (Figure 6E). This demonstrates that the electrospun membrane can both protect the islets and allow insulin release.

3.5. *In vivo* systemic toxicity and hemocompatibility

The systemic safety of the electrospun membranes was rigorously evaluated using a subcutaneous implantation model in mice. The electrospun membrane devices (approximately 1.2 cm in diameter) were surgically implanted subcutaneously into the back of healthy balb/c mice (n = 6 per group). After implantation for fourteen d, the animals were sacrificed, and major internal organs were carefully removed, sectioned, and stained with H&E for histopathological evaluation (Figure 7A). Compared with the control group (incision only without implant), no significant histopathological abnormalities were detected in any examined organs, indicating that the electrospun membranes did not cause systemic toxicity, organ damage, or non-targeted inflammatory reactions during the two-week observation period.

In addition to systemic safety, the blood compatibility of the material was assessed using a hemolysis test with fresh erythrocytes. The hemolysis rate of medical materials should be less than 5%, according to ISO 10993-5. As shown in Figure 7B, after treatment with Triton X-100, the erythrocytes completely ruptured, and the solution turned red. In contrast, the supernatants of the inner-, outer-, and dual-layer membrane extracts were colorless and transparent, consistent with the saline-treated group. Quantitative results of the absorbance of the supernatant measured at 545 nm (Figure 7C) showed that the hemolysis rates of the inner-layer membrane (4.20 ± 0.17%), outer-layer membrane (4.50 ± 0.15%), and dual-layer membrane (4.94 ± 0.12%) were all below 5%, meeting the standards for medical materials (n = 5).

4. Discussion

The transplantation of organoids and cell aggregates holds immense potential in regenerative medicine; however, clinical translation is hindered by host immune rejection and insufficient vascularization at the transplant site. This study developed a dual-layer electrospun membrane with an asymmetric pore structure designed to simultaneously address these challenges. The membrane's design draws inspiration from the structure of the natural ECM, specifically its dense basement membrane and porous interstitial matrix. The inner layer, composed of randomly oriented nanofibers with small pores (average pore size ~0.9 μm), acts as a physical size-exclusion barrier, effectively restricting the infiltration of host immune cells, which typically exceed 5–8 μm in diameter. Meanwhile, the outer layer features large pores (average pore size ~2.7 μm), a loose fibrous network, and high porosity, creating a spacious three-dimensional microenvironment that facilitates efficient mass transport. This structural anisotropy closely mimics the natural basement membrane, which serves both as a protective barrier and as a permissive matrix supporting cell survival and function.

Crucially, both layers are fabricated from the same polymer using a continuous electrospinning process, ensuring robust interlaminar adhesion. Although the pore size differential between the two layers (approximately 3-fold) is less pronounced than the gradients (approximately 6-fold) reported in certain dual-layer membrane patents, it is sufficient to achieve the intended functional compartmentalization: the inner layer provides immune protection at the cellular level, while the outer layer ensures efficient molecular exchange and permits limited host cell interaction. This design balances the competing demands inherent in cell encapsulation technology within a single, structurally simple membrane platform. Furthermore, electrospinning parameters can be independently adjusted to tune pore sizes, allowing for customization tailored to specific cell types or organoid systems with varying metabolic needs and immunogenic profiles. We plan to further optimize the concentrations and collagen ratios of the spinning solutions for both layers to achieve pore sizes in the 10–15 μm range—a size range previously reported to facilitate cell infiltration and offer pro-angiogenic potential.

Our complementary *in vitro* and *in vivo* experimental results confirm the biological relevance of this biomimetic design. The membrane extracts significantly promoted HUVEC tube formation, with both total vessel length and the number of nodes exceeding those of the control group, indicating that the material enhances *in vitro* tube formation. More importantly, supplementary *in vivo* data from rat islet transplantation provided direct functional evidence: islets encapsulated within the dual-layer membrane achieved significantly better blood glucose control compared to unencapsulated free islets. We attribute this improvement to the synergistic effect of the two layers: the dense inner layer protects islets from direct immune cell attack and excessive fibrosis, while the porous outer layer maintains islet viability through rapid glucose/insulin exchange and promotes the formation of tubular structures by surrounding endothelial cells.

Despite these promising properties, several limitations of the present study should be acknowledged. First, the 14-day subcutaneous implantation experiment provided preliminary evidence of short-term biocompatibility but was insufficient to establish the long-term stability and degradation behavior of the dual-layer membrane under

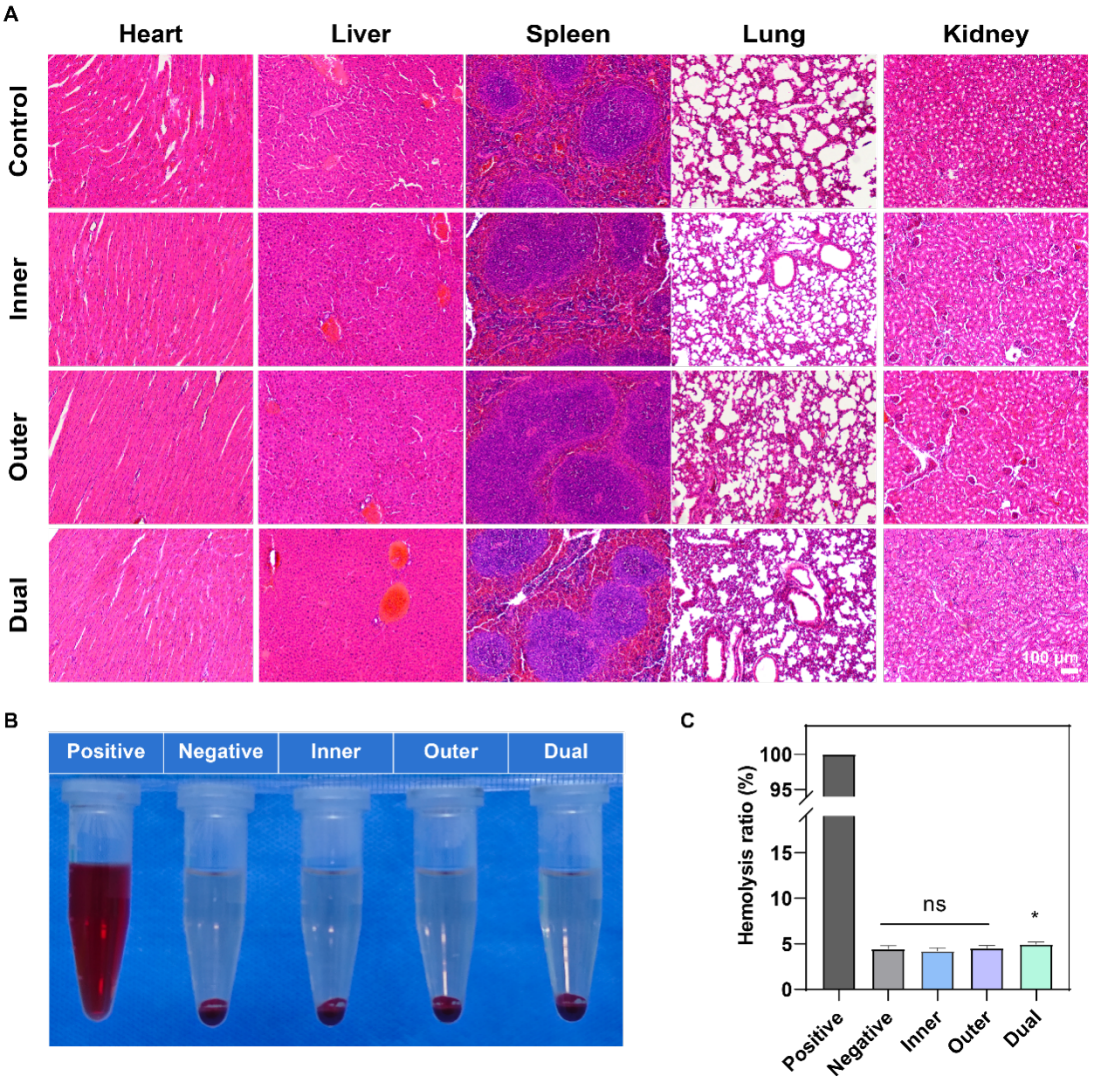

Figure 7. *In vivo* biocompatibility and hemocompatibility evaluation after subcutaneous implantation. (A) Hematoxylin-eosin staining of major organs (heart, liver, spleen, lung, kidney) after 14 days of implantation. Scale bar: 100 μm; magnification: 10×. (B) Image and (C) quantitative statistics of hemolysis experiment (n = 3).

physiological conditions. Because the membrane contains electrospun collagen, which is susceptible to enzymatic degradation, its structural integrity, degradation rate, and potential effects on membrane permeability over time require further investigation. Second, adequate vascularization is essential for maintaining the long-term survival and function of transplanted cells or organoids. Although the membrane extracts promoted HUVEC tube formation *in vitro*, this result only indicates potential pro-angiogenic activity and does not demonstrate enhanced vascularization *in vivo*. Longer-term implantation studies with histological assessment of vascular density and tissue integration are therefore needed. Third, the immune response to the implanted membrane was not comprehensively characterized in this study. Although the short-term evaluation provided preliminary biocompatibility data, the long-term local inflammatory response, macrophage infiltration, and potential fibrous capsule remain to be investigated. Future studies involving extended observation periods, systematic evaluation of membrane degradation and structural integrity, direct assessment of vascularization, and characterization of local immune responses will be necessary to determine the suitability of this membrane for long-term cell and organoid encapsulation and transplantation.

5. Conclusion

In this study, a duallayer electrospun membrane with an asymmetric pore architecture was fabricated *via* sequential electrospinning. The structure comprises a dense,

microporous inner layer serving as a physical immune barrier, and a highly porous, macroporous outer layer promoting angiogenesis and substance transport, thus mimicking the hierarchical structure of the natural ECM. The membrane exhibits excellent mechanical integrity, no interfacial delamination, superior cell compatibility, and significant pro-vascularization activity. In a diabetic mouse model with rat islets, encapsulated islets achieved superior glycemic control compared to the unencapsulated control group, demonstrating the therapeutic advantages of this dual-layer design. Notably, this electrospinning method allows for independent control of the fiber diameter and pore size of each layer, providing multiple options for tailoring barrier performance to specific cell types or organoid systems. While these results indicate the membrane's potential in organoid transplantation, further long-term implantation studies are needed to evaluate the durability of barrier function and the dynamic interaction between vascular ingrowth and immune protection. Our research provides a general, biomimetic strategy for cell encapsulation and organoid transplantation and offers a simple, adjustable approach for designing tissue-engineered scaffolds that balance physical protection and biological function.

Acknowledgments

None.

Funding

This work was supported by the National Key Research Development Program of China (2020YFA0803701), Key Projects of Science and Technology in Shenzhen (202406003), National Key Specialty Construction Project (Grant No. 2023283) and Tianjin Key Medical Discipline Construction Project (Grant No. TJYXZDXK-3-003D).

Conflict of interest

The authors declare they have no competing interests.

Author contributions

Conceptualization: Xin Yi, Xiaoming Hou
Formal analysis: Jinpeng Wan, Yiming Wang, Dan Yao
Investigation: Xin Yi, Zhihao Pan, Yukang Wang
Methodology: Zhihao Pan, Yukang Wang, Jie Wang, Yufei Liu, Jie Zhou
Writing – original draft: Xin Yi
Writing – review & editing: Yufei Liu, Shufang Wang

Ethics approval and consent to participate

All animal experiments were approved by the Animal Welfare and Ethics Review Committee of Nankai University (Approval No.: 2026-SYDWLL-000830). This study does not involve human subjects or primary cell lines derived from human patients; therefore, informed consent was not required.

Consent for publication

Not applicable.

Availability of data

The data supporting the findings of this study are available within the article and its supplementary materials. Additional data can be obtained from the corresponding author upon reasonable request.

Further disclosure

Part of the findings of this study were presented as a poster at the 9th China-Europe Symposium on Biomaterials in Regenerative Medicine (CESB 2026; May 10–13, 2026). This manuscript has not been uploaded to or deposited in any preprint server.

AI tools statement

DeepSeek (DeepSeek-AI, DeepSeek-V4.1-Flash-1017, China) and ChatGPT (OpenAI, GPT-6, USA) were used in the preparation of this manuscript to refine the text and correct grammatical and linguistic errors. All scientific content was critically reviewed and verified by the authors, who take full responsibility for the accuracy and integrity of the manuscript.

References

1. Lancaster MA, Knoblich JA. Organogenesis in a dish: Modeling development and disease using organoid technologies. *Science*. 2014;345(6194):1247125.

   doi: 10.1126/science.1247125

2. Clevers H. Modeling Development and Disease with Organoids. *Cell*. 2016;165(7):1586-1597.

   doi: 10.1016/j.cell.2016.05.082

3. Corsini NS, Knoblich JA. Human organoids: New strategies and methods for analyzing human development and disease. *Cell*. 2022;185(15):2756-2769.

   doi: 10.1016/j.cell.2022.06.051

4. Zhao J, Shen F, Sheng S, *et al.* Cartilage-on-chip for osteoarthritis drug screening. *Organoid Research*. 2025;1(1):8461.

   doi: 10.36922/or.8461

5. Kim J, Koo BK, Knoblich JA. Human organoids: model systems for human biology and medicine. *Nat Rev Mol Cell Biol*. 2020;21(10):571-584.

   doi: 10.1038/s41580-020-0259-3

6. Bai L, Jing Y, Reis RL, Chen X, Su J, Liu C. Organoid research: Theory, technology, and therapeutics. *Organoid Research*.

2025;1(1):025040007.

doi: 10.36922/OR025040007

7. Yu X, Liu C, Kuang Z, Song S, Tian L, Wang Y. Islet organoids: a new hope for islet transplantation in diabetes. *Front Immunol*. 2025;15:1540209.

doi: 10.3389/fimmu.2024.1540209

8. Takebe T, Sekine K, Enomura M, *et al.* Vascularized and functional human liver from an iPSC-derived organ bud transplant. *Nature*. 2013;499(7459):481-484.

doi: 10.1038/nature12271

9. Song S, Zhang J, Fang Y, *et al.* Nerve–bone crosstalk manipulates bone organoid development and bone regeneration: A review and perspectives. *Organoid Research*. 2025;1(1):8294.

doi: 10.36922/or.8294

10. Sun T, Feng C, Huang T, *et al.* Liver metastatic cancer organoid models: From mechanistic insights to precision medicine. *Organoid Research*. 2025;1(4):025370029.

doi: 10.36922/OR025370029

11. Yang S, Hu H, Kung H, *et al.* Organoids: The current status and biomedical applications. *MedComm*. 2023;4(3):e274.

doi: 10.1002/mco2.274

12. Park S, Cho SW. Bioengineering toolkits for potentiating organoid therapeutics. *Advanced Drug Delivery Reviews*. 2024;208:115238.

doi: 10.1016/j.addr.2024.115238

13. Yang J, Yan Y, Yin X, *et al.* Bioengineering and vascularization strategies for islet organoids: advancing toward diabetes therapy. *Metabolism*. 2024;152:155786.

doi: 10.1016/j.metabol.2024.155786

14. Zhang YS, Khademhosseini A. Advances in engineering hydrogels. *Science*. 2017;356(6337):eaaf3627.

doi: 10.1126/science.aaf3627

15. Lutolf MP, Hubbell JA. Synthetic biomaterials as instructive extracellular microenvironments for morphogenesis in tissue engineering. *Nat Biotechnol*. 2005;23(1):47-55.

doi: 10.1038/nbt1055

16. Abraham N, Kolipaka T, Pandey G, Negi M, Srinivasarao DA, Srivastava S. Revolutionizing pancreatic islet organoid transplants: Improving engraftment and exploring future frontiers. *Life Sciences*. 2024;343:122545.

doi: 10.1016/j.lfs.2024.122545

17. Kavand A, Noverraz F, Gerber-Lemaire S. Recent Advances in Alginate-Based Hydrogels for Cell Transplantation Applications. *Pharmaceutics*. 2024;16(4):469.

doi: 10.3390/pharmaceutics16040469

18. Krishnan R, Alexander M, Robles L, Foster 3rd CE, Lakey JRT. Islet and Stem Cell Encapsulation for Clinical Transplantation. *Rev Diabet Stud*. 2014;11(1):84-101.

doi: 10.1900/RDS.2014.11.84

19. Vaithilingam V, Bal S, Tuch BE. Encapsulated Islet Transplantation: Where Do We Stand. *Rev Diabet Stud*. 2017;14(1):51-78.

doi: 10.1900/rds.2017.14.51

20. Orive G, Santos E, Poncelet D, *et al.* Cell encapsulation: technical and clinical advances. *Trends in Pharmacological Sciences*. 2015;36(8):537-546.

doi: 10.1016/j.tips.2015.05.003

21. Scharp DW, Marchetti P. Encapsulated islets for diabetes therapy: History, current progress, and critical issues requiring solution. *Advanced Drug Delivery Reviews*. 2014;67-68:35-73.

doi: 10.1016/j.addr.2013.07.018

22. Levey RE, Coulter FB, Scheiner KC, *et al.* Assessing the Effects of VEGF Releasing Microspheres on the Angiogenic and Foreign Body Response to a 3D Printed Silicone-Based Macroencapsulation Device. *Pharmaceutics*. 2021;13(12):2077.

doi: 10.3390/pharmaceutics13122077

23. Desai T, Shea LD. Advances in islet encapsulation technologies. *Nat Rev Drug Discov*. 2017;16(5):338-350.

doi: 10.1038/nrd.2016.232

24. Zhang Y, Zhang C, Li Y, *et al.* Evolution of biomimetic ECM scaffolds from decellularized tissue matrix for tissue engineering: A comprehensive review. *International Journal of Biological Macromolecules*. 2023;246:125672.

doi: 10.1016/j.ijbiomac.2023.125672

25. Phelps EA, Templeman KL, Thulé PM, García AJ. Engineered VEGF-releasing PEG-MAL hydrogel for pancreatic islet vascularization. *Drug Deliv Transl Res*. 2015;5:125-136.

doi: 10.1007/s13346-013-0142-2

26. Theocharis AD, Skandalis SS, Gialeli C, Karamanos NK. Extracellular matrix structure. *Advanced Drug Delivery Reviews*. 2016;97:4-27.

doi: 10.1016/j.addr.2015.11.001

27. Huch M, Koo BK. Modeling mouse and human development using organoid cultures. *Development*. 2015;142(18):3113-3125.

doi: 10.1242/dev.118570

28. Badylak SF, Freytes DO, Gilbert TW. Extracellular matrix as a biological scaffold material: Structure and function. *Acta Biomaterialia*. 2009;5(1):1-13.

doi: 10.1016/j.actbio.2008.09.013

29. Xue J, Wu T, Dai Y, Xia Y. Electrospinning and Electrospun Nanofibers: Methods, Materials, and Applications. *Chem Rev*. 2019;119(8):5298-5415.

doi: 10.1021/acs.chemrev.8b00593

30. Ding J, Zhang J, Li J, *et al.* Electrospun polymer biomaterials. *Progress in Polymer Science*. 2019;90:1-34.

    doi: 10.1016/j.progpolymsci.2019.01.002

31. Liu H, Ding X, Zhou G, Li P, Wei X, Fan Y. Electrospinning of Nanofibers for Tissue Engineering Applications. *Journal of Nanomaterials*. 2013;2013:495708.

    doi: 10.1155/2013/495708

32. Sill TJ, von Recum HA. Electrospinning: Applications in drug delivery and tissue engineering. *Biomaterials*. 2008;29(13):1989-2006.

    doi: 10.1016/j.biomaterials.2008.01.011

33. Jin G, Prabhakaran MP, Ramakrishna S. Stem cell differentiation to epidermal lineages on electrospun nanofibrous substrates for skin tissue engineering. *Acta Biomaterialia*. 2011;7(8):3113-3122.

    doi: 10.1016/j.actbio.2011.04.017

34. Gupta KC, Haider A, Choi Y, Kang IK. Nanofibrous scaffolds in biomedical applications. *Biomaterials Research*. 2014;18(1):5.

    doi: 10.1186/2055-7124-18-5

35. Colton CK. Implantable biohybrid artificial organs. *Cell Transplantation*. 1995;4(4):415-436.

    doi: 10.1016/0963-6897(95)00025-S

36. Avgoustiniatos ES, Colton CK. Effect of External Oxygen Mass Transfer Resistances on Viability of Immunoisolated Tissue. *Annals of the New York Academy of Sciences*. 1997;831(1):145-167.

    doi: 10.1111/j.1749-6632.1997.tb52192.x

37. Lanza RP, Hayes JL, Chick WL. Encapsulated cell technology. *Nat Biotechnol*. 1996;14(9):1107-1111.

    doi: 10.1038/nbt0996-1107

38. Laschke MW, Menger MD. Vascularization in Tissue Engineering: Angiogenesis versus Inosculation. *Eur Surg Res*. 2012;48(2):85-92.

    doi: 10.1159/000336876

39. Stachewicz U, Szewczyk PK, Kruk A, Barber AH, Czyrska-Filemonowicz A. Pore shape and size dependence on cell growth into electrospun fiber scaffolds for tissue engineering: 2D and 3D analyses using SEM and FIB-SEM tomography. *Materials Science and Engineering: C*. 2019;95:397-408.

    doi: 10.1016/j.msec.2017.08.076

40. Khademhosseini A, Langer R. A decade of progress in tissue engineering. *Nat Protoc*. 2016;11(10):1775-1781.

    doi: 10.1038/nprot.2016.123

41. Jin Y, Chen Q, Gong L, *et al.* Organoids: Applications and challenges of advanced hydrogels in tissue systems. *Organoid Research*. 2025;1(2):8262.

    doi: 10.36922/or.8262

42. Vegas AJ, Veiseh O, Doloff JC, *et al.* Combinatorial hydrogel library enables identification of materials that mitigate the foreign body response in primates. *Nat Biotechnol*. 2016;34(3):345-352.

    doi: 10.1038/nbt.3462

43. Bochenek MA, Veiseh O, Vegas AJ, *et al.* Alginate encapsulation as long-term immune protection of allogeneic pancreatic islet cells transplanted into the omental bursa of macaques. *Nat Biomed Eng*. 2018;2(11):810-821.

    doi: 10.1038/s41551-018-0275-1

44. Mei QJ, Wen JQ, Xu XX, Xie HQ. Generation of vascularized brain organoids: Technology, applications, and prospects. *Organoid Research*. 2025;1(2):8162.

    doi: 10.36922/or.8162

45. Farina M, Alexander JF, Thekkedath U, Ferrari M, Grattoni A. Cell encapsulation: Overcoming barriers in cell transplantation in diabetes and beyond. *Advanced Drug Delivery Reviews*. 2019;139:92-115.

    doi: 10.1016/j.addr.2018.04.018

46. Zhou Z, Li R, Ding X, Li Y, Luo Y, Liang S. Digital light processing-printed macroencapsulated human liver organoids preserve hepatic stellate cell quiescence for transplantation in immunocompetent mice. *Int J Bioprint*. 2026;12(3):026140130.

    doi: 10.36922/IJB026140130

47. Wang H, Duan C, Luo R, *et al.* A Pro-Angiogenic Immunoprotective Membrane for Cell Therapies. *Advanced Healthcare Materials*. 2025;14(1):2400459.

    doi: 10.1002/adhm.202400459

48. Pham TT, Tran PL, Tempelman LA, *et al.* A continuously oxygenated macroencapsulation system enables high-density packing and delivery of insulin-secreting cells. *Nat Commun*. 2025;16(1):7199.

    doi: 10.1038/s41467-025-62271-2

49. Krishnan L, Clayton LR, Boland ED, Reed RM, Hoying JB, Williams SK. Cellular immunoisolation for islet transplantation by a novel dual porosity electrospun membrane. *Transplant Proc*. 2011;43(9):3256-3261.

    doi: 10.1016/j.transproceed.2011.10.031

50. Bružauskaitė I, Bironaitė D, Bagdonas E, Bernotienė E. Scaffolds and cells for tissue regeneration: different scaffold pore sizes—different cell effects. *Cytotechnology*. 2016;68(3):355-369.

    doi: 10.1007/s10616-015-9895-4

51. Omachi K, Fujiwara H. Exploring basement membrane dynamics through cross-scale imaging, manipulation, and molecular mapping. *Matrix Biology*. 2025;141:67-81.

    doi: 10.1016/j.matbio.2025.09.001

52. Mun J, Pack SP, Lee H. Fabrication and characterization of electrospun polycaprolactone/Urechis unicinctus derived-ECM composite scaffolds for small-diameter vascular grafts. *RSC Adv*. 2025;15(38):31060-31075.

doi: 10.1039/d5ra04406e

53. Pang X, Li W, Chang L, Gautrot JE, Wang W, Azevedo HS. Hyaluronan (HA) Immobilized on Surfaces via Self-Assembled Monolayers of HA-Binding Peptide Modulates Endothelial Cell Spreading and Migration through Focal Adhesion. *ACS Appl Mater Interfaces*. 2021;13(22):25792-25804.

doi: 10.1021/acsami.1c05574

54. He X, Li W, Liu S, *et al.* Fabrication of high-strength, flexible, porous collagen-based scaffolds to promote tissue regeneration. *Materials Today Bio*. 2022;16:100376.

doi: 10.1016/j.mtbio.2022.100376

55. Ying P, Jin G, Tao Z. Competitive adsorption of collagen and bovine serum albumin—effect of the surface wettability. *Colloids and Surfaces B: Biointerfaces*. 2004;33(3-4):259-263.

doi: 10.1016/j.colsurfb.2003.10.015

56. Upreti T, Wolfe KM, Van Bavel N, Anikovskiy M, Labouta HI. Collagen – a newly discovered major player in protein corona formation on nanoparticles. *Phys Chem Chem Phys*. 2022;24(9):5610-5617.

doi: 10.1039/d1cp03968g